PREPARATION OF A POROUS BIOCHAR FROM THE ACID ACTIVATION OF PORK BONES

Unai Iriarte-Velasco[a], Irene Sierra[a*], Lorena Zudaire[a] and Jose L. Ayastuy[b]

[a] *Department of Chemical Engineering, Faculty of Pharmacy, University of the Basque Country UPV/EHU, Paseo de la Universidad, 7, 01006 Vitoria, Spain.*

[b] *Department of Chemical Engineering, Faculty of Science and Technology, University of The Basque Country UPV/EHU, Barrio Sarriena, s/n, 48940 Leioa, Spain.*

*Corresponding author. Tel.: +34 945013290; fax: +34 946015963. E-mail: irene.sierra@ehu.eus

Abstract

A porous biochar was manufactured through the valorisation of waste pork bones, following a three-step process including pre-charring under mild conditions, acid treatment and thermal activation. The influence of the acid (H_2SO_4 and H_3PO_4) and the impregnation ratio on the physicochemical properties of the material was investigated. Acid treatment at 0.2 $mmol_{acid}/g_{precursor}$ increased BET area by about 80%, compared to untreated bone char. When using H_2SO_4, higher impregnation ratios significantly enhanced microporosity (up to 263%). This increased microporosity should be associated to a specific reaction mechanism of H_2SO_4 with a source of carbon. On the contrary, the higher activity of H_3PO_4 led to a dramatic removal of porosity for large impregnation ratios (about 20 mmol/g). The acid activation mechanism involves the formation of cation-deficient HAp, which is thereafter decomposed upon thermal treatment. The maximum uptake of methylene blue was achieved at low impregnation ratios (0.2 and 1.0 mmol/g), and could be related to surface area corresponding to large micropores and small mesopores.

KEYWORDS: bone char; biochar; acid activation; activation mechanism; adsorption

1. Introduction

The use of meat and bone meal (MBM) to feed cattle was forbidden in EU (Commission Decision 94/381/EC), as a result of Bovine Spongiform Encephalopathy crisis. Consequently, there is a high amount of animal food wastes that must be safely disposed or transformed. One of the most reliable methods for the valorisation of animal bones is pyrolysis. The solid fraction obtained (bone char) contains about 70–76 wt% calcium hydroxyapatite (HAp), $Ca_{10}(PO_4)_6(OH)_2$, 10 wt% carbon, 8 wt% $CaCO_3$ and other minor constituents (C. W. Cheung, Chan, Porter, & McKay, 2001).

Nowadays, there is a growing research interest for the use of materials based on bone char. The organic content of bones represents a source of carbon, whereas HAp acts as a natural template for the formation of a hierarchical porous structure (Wei et al., 2011), thus resulting in biochars of adequate textural properties for different applications. Bone char is a suitable material for the removal of pollutants, partly owing to the low water solubility and high ion exchange capacity of its major constituent, HAp (Arvanitoyannis & Ladas, 2008).

Bone char-derived materials have been successfully used in catalysis (Obadiah, Swaroopa, Kumar, Jeganathan, & Ramasubbu, 2012), electrochemistry (Goodman et al., 2013) and as highly specific materials for the removal of both gaseous (Cascarosa, de Zarate, Sanchez, Gea, & Arauzo, 2012; Medellin-Castillo et al., 2014; Rezaee, Ghanizadeh, Behzadiyannejad, Yazdanbakhsh, & Siyadat, 2009) and liquid pollutants (C. W. Cheung, Chan, Porter, & McKay, 2001; U. Iriarte-Velasco, Sierra, Cepeda, Bravo, & Ayastuy, 2015; Šljivić-Ivanović et al., 2015).

The applicability of bone char is strongly dependent on its porous structure. The development of porosity of a given precursor requires either chemical (Goodman et al., 2013) or physical activation (Jimenez-Cordero, Heras, Alonso-Morales, Gilarranz, & Rodriguez, 2013). Chemical activation has been reported as more advantageous than physical activation, since it results in higher yield and surface area and better development of porous structures in the resultant product (Lillo-Ródenas, Cazorla-Amorós, & Linares-Solano, 2003; Phan et al., 2006). Moreover, the temperatures used in chemical activation are lower than those required

for physical activation. Its main drawback is the need to wash to remove the residual inorganic material.

The most commonly used agents for chemical activation include inorganic salts such as $ZnCl_2$ and K_2CO_3, alkali hydroxides such as KOH and NaOH, and inorganic acids such as H_2SO_4, H_3PO_4, HNO_3 and HCl. Several attempts have been done to prepare porous materials from animal bones by chemical activation. Dimovic, Smiciklas, Plecas, Antonovic, & Mitric (2009) studied the physicochemical properties of bovine bones chemically activated with H_2O_2. Wei et al. (2011) prepared a hierarchical porous material derived from pig bone char activated by KOH. Gumus, Wauton, & Aliu (2012) and Yusufu, Ariahu, & Igbabul (2012) investigated the acid activation of cow bones, using HCl and HNO_3, and H_3PO_4, respectively. In a previous work we studied the physicochemical properties of biochars derived from pork bones prepared by alkaline treatment with NaOH, KOH and K_2CO_3 (U. Iriarte-Velasco, Sierra, Zudaire, & Ayastuy, 2015).

Acid activation is a promising treatment, since it has been successfully used to generate porosity in other waste materials, such as agroalimentary wastes (Moreno-Castilla, Carrasco-Marin, Lopez-Ramon, & Alvarez-Merino, 2001; Njoku & Hameed, 2011; Reffas et al., 2010). Nevertheless, the literature concerning the preparation of porous materials by the acid activation of animal bones is scarce, and there are important gaps in the fundamentals of the process, regarding the reaction mechanism occurring during the activation process, and its effect on the properties of the material.

In this study, pork bones were selected because, to our knowledge, there is no comprehensive report on the acid activation of pork bones in the open literature. Pork is the most consumed meat in Spain, with around 2.3 Mt in 2014 (Ministry of Agriculture, Food and Environment, 2015). Spain is the second pig meat producer in EU (3.5 Mt produced in 2014). Therefore, pork bone could represent a locally available and abundant food waste for the production of porous materials.

This paper approaches the preparation of porous materials from the acid activation of waste pork bones. The influence of both the type of acid (H_2SO_4 and H_3PO_4) and the impregnation ratio on the physicochemical properties of the final material was investigated. Furthermore, the pyrolysis products of acid impregnated samples were analysed, in order to gain knowledge

on the activation mechanism. These results are of great interest to optimize the preparation method, in order to achieve a material with the desired textural properties. Finally, the performance of the materials in the removal of methylene blue (representative for the aqueous removal of organics) was studied.

2. Experimental

2.1. Production of bone char

Samples of bone char (BC) were prepared from pork chop bones collected from a local butcher shop. The preparation protocol was as follows: first, bones were cleaned from meat and cut into pieces of 2 – 5 cm. In order to remove meat and fat, prior to chemical activation bones were precarbonized at 450 ºC in nitrogen atmosphere. From now on, precarbonized sample will be referred as precursor. Precarbonization was performed using a heating rate of 10 ºC/min until the desired temperature was reached; temperature was then held constant for 1 hour. Nitrogen flow was set at 120 cm^3/min, which corresponds to a residence time of 8 minutes in furnace. Precarbonized samples were left to cool down in nitrogen atmosphere.

The precursor was sieved and particles in the 0.25 – 0.35 mm size range were selected. It was then divided into four parts. Two were impregnated with either H_3PO_4 (P) or H_2SO_4 (S) and pyrolysed. The third part was pyrolysed without chemical treatment (O), and the last part was no further modified to be used as a reference. For the impregnation step about 2 g of precursor were contacted with 40 cm^3 of a solution containing the activating agent. Solutions were stirred at room temperature (20 ± 2 ºC) for 24 h. Samples were then filtered, transferred to a convection oven and dried at 80 C for 24 hours. The pyrolysis step was conducted at 800 ºC under operating conditions similar to those used during the precarbonization stage. Samples of bone char were washed with distilled water until neutral pH of solution was reached.

The effect of the impregnation ratio was studied at three levels: 20, 1.0 and 0.2 $mmol_{agent}/g_{precursor}$. The adsorbents prepared at the maximum impregnation ratio were coded indicating the activation agent used; BCO, BCS, BCP. The materials prepared at lower impregnation ratios (1.0 and 0.2 mmol/g) were coded as BCr1.0 and BCr0.2, respectively.

2.2. Physical and chemical characterization

The textural properties of the materials were measured by nitrogen adsorption-desorption at 77 K using a porosimeter (ASAP 2010, Micromeritics). Prior to the measurements samples were dried and outgassed at 200 °C under a nitrogen flow for 15 hours. Brunauer, Emmett & Teller (BET), t-plot, density functional theory (DFT) and Barrett, Joyner & Halenda (BJH) methods were used.

The point of zero charge (pH_{PZC}) was determined following the method proposed by Babic, Milonjic, Polovina, & Kaludierovic (1999). About 20 cm^3 of a 0.01 N KCl-0.004 N KOH solution were contacted with 0.1 g of bone char. This solution was titrated with a 0.1 N HCl solution. The titrating solution was added slowly (0.1 cm^3 every 10 min) and data of both the volume of the titrating solution added and the solution pH were recorded. On the other hand, the KCl-KOH solution was also titrated without bone char under the same operating conditions. The pH_{PZC} is the pH at which the titration curve with bone char intersects the titration curve without bone char.

In order to investigate the reactions that take place during the activation process, thermogravimetric (TG) analysis was coupled to mass spectrometry (MS). TG analyses were performed with a Setsys evolution (Setaram) thermal analyser. About 70 mg of sample (impregnated precursor) were put into the alumina crucible and heated under helium atmosphere from room temperature to 1000 ºC at a heating rate of 10 ºC/min. The thermal analyser exhaust gases were monitored on-line by a mass spectrometer (MKS, Cirrus 3000). The following compounds were collected continuously: H_2O (m/z = 18) and CO_2 (m/z = 44).

The chemical composition and surface properties of the materials were analysed by a scanning electron microscope (JEOL JSM-7000F) equipped with energy dispersive X-ray detector (EDX). Fourier-transformed infrared (FTIR) spectra were collected with a Nicolet Protégé 460 device in the transmittance mode, in the 400-4000 cm^{-1} with a resolution of 2 cm^{-1}. Spectra were obtained using the KBr self-supported pellet technique. The X-ray powder diffraction (XRD, PANalytical Xpert PRO) analyses were performed with CuKα radiation (λ = 1.5418 Å) in continuous scan mode in the 5-70º 2θ range, with a 0.02º step size. The analysis of the diffraction peaks was performed using PANalytical Xpert HighScore software.

2.3. Adsorption tests

Methylene blue (MB) was selected as model adsorbate not only because of its environmental concern but also because it has been recognized as a valid representative solute for the removal of organics (Rafatullah, Sulaiman, Hashim, & Ahmad, 2010). About 10 mg of the prepared materials were contacted in stoppered glass vials with 10 cm^3 of aqueous solutions of methylene blue with known concentration. The adsorption experiments were carried out at 20 ± 0.5 ºC in a rotary mixer placed in a thermostatic chamber, being the initial pH of the solutions 5.8. Samples were centrifuged and the residual concentration of the solute in the supernatant was analysed. The concentration of MB was measured by UV/VIS spectrophotometry (Jasco V-630), recording UV absorbance at a wavelength of 664 nm.

The amount of solute adsorbed per mass of adsorbent was calculated by mass balance:

$$q_t = (C_o - C_t)\frac{V}{m} \quad (1)$$

where C_o and C_t are the liquid phase solute concentrations at initial and t contact time, respectively; V is the solution volume, and m the adsorbent mass.

For the collection of isotherm data, an aliquot of 2 cm^3 of supernatant solution was removed every 48 hours and MB concentration was measured. It was then replaced by 2 cm^3 of 50 mg/L MB stock solution. The adsorbed solute per mass of solid in the subsequent steps of isotherm construction was determined by mass balance.

Equilibrium data were fitted to Freundlich (Eq. 2) and Langmuir equations (Eq. 3). The best fitting parameters were calculated by non linear regression.

$$q_e = K_F C_e^{1/n_F} \quad (2)$$

$$q_e = \frac{Q_L K_L C_e}{1 + K_L C_e} \quad (3)$$

The goodness of fit of each model was determined by means of the root mean square error (RMSE):

$$RMSE = \sqrt{\frac{\sum_{i=0}^{i=n}\left(q_{\exp} - q_{est}\right)^2}{n}} \quad (4)$$

where q_{exp} is the experimentally measured uptake capacity; q_{est} is the model predicted uptake capacity, and n is the number of experiments used for model development.

The intraparticle effective diffusivity (D_{eff}) was estimated from the slope of Eq. 5.

$$\frac{q}{q_e} = 6\sqrt{\frac{D_{eff}}{R^2\pi}}t^{0.5} = k_d t^{0.5} \quad (5)$$

3. Results and Discussion

3.1. Production yield

The total yield (Y_T), chemical impregnation yield (Y_{Chem}) and thermal activation yield (Y_{Therm}) were calculated according to the following equations:

$$\mathrm{Y_T} = \frac{\mathrm{BC}}{\mathrm{P}} \quad (6)$$

$$\mathrm{Y_{Chem}} = \frac{\mathrm{IP}}{\mathrm{P}} \quad (7)$$

$$\mathrm{Y_{Therm}} = \frac{\mathrm{BC}}{\mathrm{IP}} \quad (8)$$

where BC is the weight of the final product (BCO, BCP, BCS); P refers to the weight of the precursor (precarbonized bone), and IP is the weight of the impregnated precursor (before being carbonized at 800 ºC).

Data in Table 1 show that Y_T and Y_{Therm} decreased for chemically activated samples as compared to non chemically treated sample (BCO), which showed the maximum total yield, with about 68% of initial precursor converted into bone char. H_3PO_4 caused the most significant weight loss during the chemical impregnation (more than 80% weight loss of the initial precursor, Y_{Chem}=18.9), much more pronounced than H_2SO_4, which resulted in about 30% weight loss (Y_{Chem}=69.8). During the carbonization step, both acids led to a similar weight loss, about 50%. Regarding the overall preparation process, the production yield was

minimum for H_3PO_4 activation (about 9% of the precursor was transformed into the final product), while H_2SO_4 treatment achieved 40%.

Table 1. Total yield and partial yields of different preparation steps: chemical impregnation and thermal treatment.

Sample	Y_{Chem} (%)	Y_{Therm} (%)	Y_T (%)
BCO	-	68.3	68.3
BCP	18.9	47.9	9.1
BCS	69.8	56.6	39.5

3.2. Textural and chemical properties

3.2.1. Specific surface area and total pore volume

The textural properties of the prepared materials, measured by BET, t-plot, DFT and BJH methods, are summarized in Table 2. The specific surface area and pore volume varied significantly depending on the acid and impregnation ratio used. H_2SO_4 treated samples showed the largest BET surface areas (116.8 – 139.6 m^2/g) with up to 83% increase compared to non activated BCO sample (76.2 m^2/g). The BET surface area of the prepared materials was maximum at the lowest impregnation ratio (0.2 mmol/g), being about twice of the non acid treated sample. When using H_2SO_4 as activation agent, BET specific surface area slightly decreased when the impregnation ratio was increased. On the contrary, when chemical activation was carried out with H_3PO_4, BET surface area was dramatically decreased as impregnation ratio increased. For the latter, at the lowest impregnation ratio of 0.2 mmol/g, S_{BET} was 136.4 m^2/g, and at 20 mmol/g a sharp drop-off occurred, leading to a S_{BET} of only 3.2 m^2/g.

Table 2. Textural properties of prepared bone chars. Surface area in m^2/g; pore volume in cm^3/g; average pore diameter, D_p in Å.

Sample	S_{BET}	S_{micro} (a)	S_{ext} (a)	S_{eff} (b)	V_p (c)	D_p (d)
BCO	76.2	14.1	62.1	35.0	0.265	107.3
BCS						
r = 20 mmol/g	116.8	51.2	65.6	32.2	0.139	85.7
r = 1.0 mmol/g	121.2	24.7	96.5	51.1	0.310	89.9
r = 0.2 mmol/g	139.6	23.5	116.1	67.2	0.279	74.1
BCP						
r = 20 mmol/g	3.2	n.d	n.d.	3.6	0.006	53.0
r = 1.0 mmol/g	61.9	14.3	47.7	36.6	0.179	83.4
r = 0.2 mmol/g	136.4	15.7	120.7	58.1	0.323	72.8

a) t-plot
b) BJH method (1.7 nm < D_p > 5.0 nm).
c) Sum of DFT method (D_p < 1.7 nm) and BJH method (D_p >1.7 nm).
d) BJH method, desorption branch.

In order to distinguish between micropore (S_{micro}) and external surface area (sum of meso- and macroporosity) (S_{ext}), the t-plot-method proposed by Harkins and Jura was used. The value of S_{ext} followed a progressive decrease as the applied H_2SO_4 impregnation ratio was increased. Regarding the effect on S_{micro}, it was observed that at the highest impregnation ratio, H_2SO_4 treatment significantly developed microporosity on bone char, as revealed by the 263% increase in S_{micro} compared to BCO, and by the reduction of the average pore size from 10.7 to 8.6 nm. That is, H_2SO_4 led to an opposite trend in S_{micro}, compared to the aforementioned effect on the external surface area. As a result, the activation with sulphuric acid caused a trade off between external and micropore area.

The activation with H_3PO_4 had a different effect. For the lowest impregnation ratio (0.2 mmol/g), it resulted in an increase in external area (94%), whereas it had almost no effect on micropore area. When increasing the impregnation ratio up to 1.0 mmol/g, S_{ext} was reduced, while S_{micro} remained almost unchanged. For the highest impregnation ratio (20 mmol/g), the porosity of the resultant material was dramatically reduced, as evidenced by the lowering of

pore volume to 0.006 cm^3/g and the supression of S_{micro}, S_{ext} and BET area. In general, independent of the activation agent used, the highest values of total pore volume and BET area were measured for samples treated at low impregnation ratios (0.2 and 1.0 mmol/g).

3.2.2. Pore distribution

Chemical activation led to important alterations in the pore distribution of the resulting char, as shown in Figure 1. BCO showed a multimodal pore distribution with five main peaks with their maximum at 0.7, 0.9, 1.1, 3.6, 9.0 nm and a wide band in the 18.2 to 50 nm range. At an impregnation ratio ≤ 1.0 mmol/g, sulphuric and phosphoric acid activation maintained the meso- and macropore distribution whereas new pores were created in the micropore range (d_p < 2 nm). At an impregnation ratio of 20 mmol/g, H_2SO_4 activated sample maintained a multimodal pore distribution in the micropore range (new pores were created mainly at 2.0 nm and between 0.6 and 1.4 nm), while macropores were cleared.

On the contrary, at the same impregnation ratio, H_3PO_4 dramatically reduced pore volume and surface area throughout all pore sizes, which is in good agreement with the results in section 3.2.1. This destructive effect was accompanied by a severe mass loss (Table 1). Although the maximum impregnation ratio used in this work (20 mmol/g) was within the normal range used for the acid activation of lignocellulosic (Moreno-Castilla et al., 2001; Puziy, Poddubnaya, Martínez-Alonso, Suárez-García, & Tascón, 2003) and biomass waste materials (Izquierdo, Martínez de Yuso, Rubio, & Pino, 2011), the results of samples activated with H_3PO_4 evidence that lower ratios are required for the activation of bones. The high activity of this acid led to a dramatic removal of porosity, due to the collapse of pore walls in the structure.

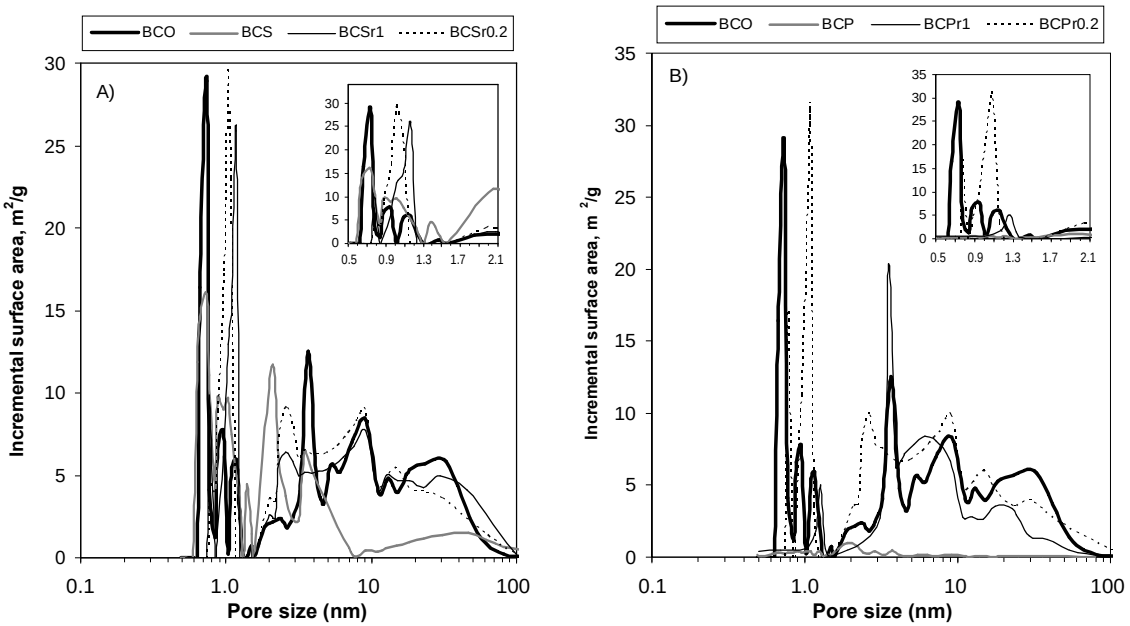

Figure 1. Pore distribution of acid treated bone chars. a) Treatment with sulphuric acid; b) Treatment with phosphoric acid.

3.2.3. Chemical composition

The SEM images of the precursor and acid activated samples are shown in Figure 2. Figures 2A,D,G show the SEM images of non activated bone char (precursor). It is observed that particles have irregular shape and a multilayered structure. The surface shows some cavities in the micron range, mainly in the rupture surfaces generated during the grinding of bones.

The SEM images of H_2SO_4 activated sample are shown in Figures 2B,E,H. It is evident that the chemical activation with H_2SO_4 does not significantly affect the surface of bone char, since the morphology and texture do not change. However, activation with H_2SO_4 smoothed the surface of the particles and reduced the number of cavities (Figures 2E,H).

Figures 2C,F,I display the SEM images of H_3PO_4 activated samples. Activation with H_3PO_4 caused a significant cracking of precursor particles. Figure 2C reveals the presence of a large number of small particles, which cover the natural cavities of the precursor. The morphology of the surface is completely different, and it is clear that the activation with H_3PO_4 damaged the surface of the particles.

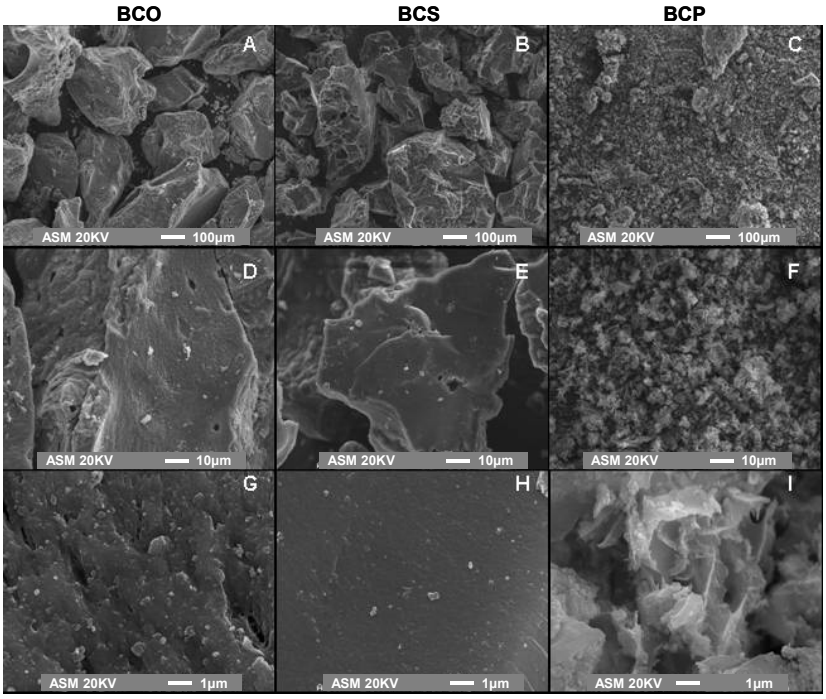

Figure 2. SEM images of the prepared bone chars.

Local EDX analyses (Fig. 3 and Table 3) reveal that the matrix is rich in calcium, oxygen, phosphorus and carbon, with small amounts of Cl, K, Mg, S and Na. It is noteworthy the high carbon content of the precursor (precarbonized bone), revealing that its content of organic matter is still high. A Ca/P molar ratio of 1.64 is measured for both the precursor and non acid treated sample (BCO), indicating that the thermal treatment does not substantially modify the Ca/P ratio. This value is slightly lower than the stoichiometric value of pure hydroxyapatite (1.67), and decreases to 1.05 and 0.54 for BCP and BCS, respectively. This low Ca/P value (very far from that of HAp) suggests that other compounds (such as calcium sulphate) coexist with hydroxyapatite in the solid phase. A concomitant increase of sulphur (from 0.13% in BCO to 1.45% in BCS) and phosphorus (from 11.5% in BCO to 16.9% in BCP) is observed.

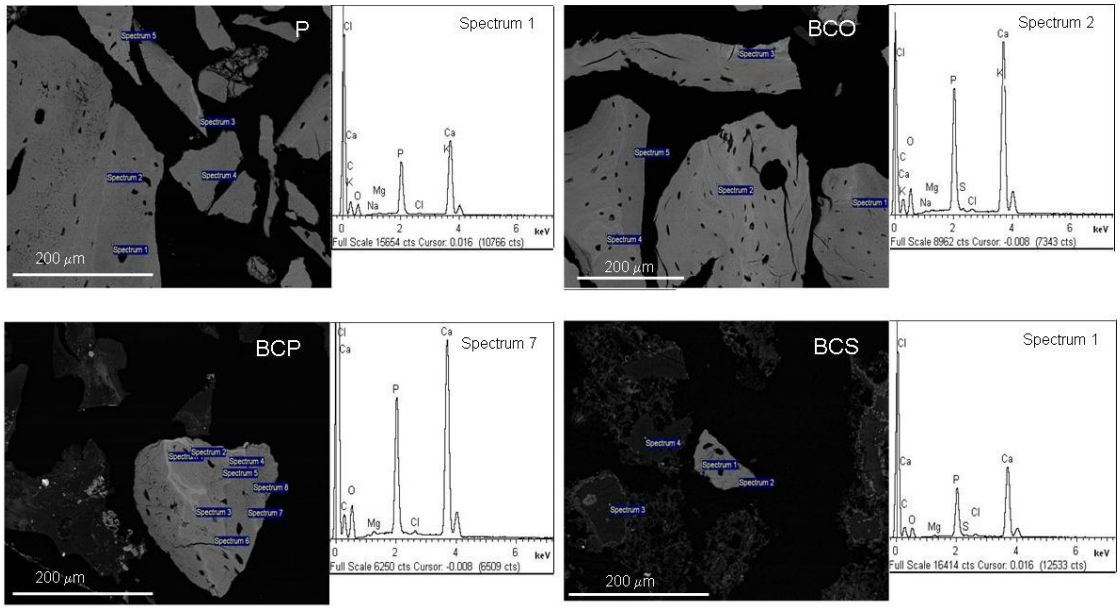

Figure 3. Local EDX spectra of prepared bone chars.

Table 3. Summary of SEM-EDX elemental analysis of HAp-based samples. Results in % in mass, except for Ca/P ratio.

Sample	C	P	S	Ca	Ca/P (molar ratio)
Precursor	27.0	13.5	0.19	28.6	1.64
BCO	38.0	11.5	0.13	24.2	1.63
BCS	39.6	15.0	1.45	10.6	0.54
BCP	26.2	16.9	0.07	22.9	1.05

The FTIR spectra of the prepared samples, shown in Figure 4, reveal the presence of phosphate groups in the precursor and BCO samples. Phosphate stretching bands are observed at around 1041 and 961 cm^{-1}, while the bending vibrations of these functional groups are observed as a strong peak located at 603 cm^{-1} (Reyes-Gasga et al., 2013). In addition, the P-O mode is visible at 706 cm^{-1} (Zendah, Khattech, & Jemal, 2013) for those samples. The signal at 875 cm^{-1} cannot be unambiguously ascribed, since the P-O stretching vibration (Bamzai, Suri, & Singh, 2012) and the bending mode of carbonate group (Giardina & Fanovich, 2010)

overlap at this wave number. The samples treated with H_2SO_4 and H_3PO_4 exhibit several bands, ascribed to phosphate groups. The presence of CO_3^{2-} ions is also clearly visible for the precursor and BCO, as deduced from the bands at 1420–1463 cm^{-1} of the C–O stretching mode of carbonate. There is an absence of carbonate bands in the spectra of acid treated samples.

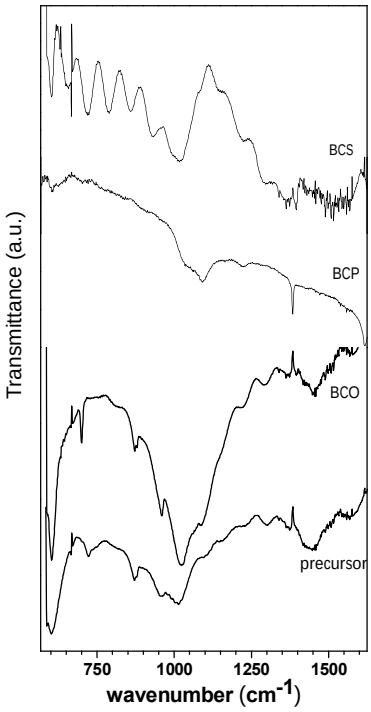

Figure 4. FTIR spectra of the precursor and acid treated samples.

The XRD patterns (Figure 5) show the characteristic peaks of HAp for all samples (precursor, BCO and BCS) except for BCP. The thermal activation increases the crystallinity, since BCO shows narrower peaks and increased intensity, compared to the precursor. The peak at 2θ= 29.1º evidences the existence of calcium carbonate in BCO sample. This component was partly removed by sulphuric acid, as deduced from the XRD pattern of BCS. The treatment with sulphuric acid results in a slight change in the crystallinity of the material, presumably because of the presence of other solid compounds, such as calcium sulphate. The activation with H_3PO_4 causes an important reduction of crystallinity (BCP shows a wide band centred at 25.5º). According to Krupa-Żuczek, Kowalski, & Wzorek (2008), mild concentrations of acid would lead to the partial dissolution of HAP, resulting in a solid phase composed of HAP and

$CaPO_3(OH)\cdot 2H_2O$. Other authors have reported the presence of various phosphates ($CaHPO_4\cdot 2H_2O$, $Ca(H_2PO_4)_2\cdot H_2O$ and $Ca_3(PO_4)_2$), after acid and heat treatment (Kon, Hirakata, Miyamoto, Kawano, & Asaoka, 2002). The wide band observed in the XRD pattern could be ascribed to the coalescence of those peaks.

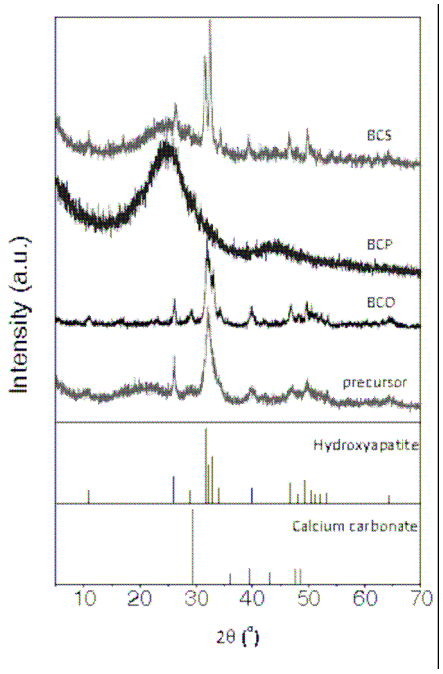

Figure 5. XRD patterns for the precursor and acid treated samples.

pH_{PZC} was measured in order to analyse surface chemistry upon activation. Untreated bone char (BCO) recorded the highest values of pH_{PZC} (7.8) followed by BCS (6.5). Treatment with phosphoric acid resulted in a bone char with the most acidic surface (pH_{PZC} = 4.6). The basic and acid sites are formed by the protonation and deprotonation of the hydroxyapatite surface hydroxyl groups, as follows:

$$Ca - OH + H^+ \leftrightarrow Ca - OH_2^+ \quad (9)$$

$$P - OH \leftrightarrow PO^- + H^+ \quad (10)$$

The acidic properties of BCP might be related to phosphorus-containing compounds formed during carbonization, possibly polyphosphates. Some of the oxygenated groups attached to carbon, such as carboxylic and/or phenolic groups, may be responsible for surface acidity.

However, this hypothesis could not be confirmed by FTIR data (Fig. 3). Although most of the acidic oxygen-containing groups are known to decompose at temperatures above 250 ºC (De la Puente, Pis, Menéndez, & Grange, 1997), and thus would not withstand carbonization at 800 ºC, some acidic groups might be formed by oxidation, after the cooled samples were exposed to air. It should be stressed that all adsorbents were extensively washed in fixed bed with 600 bed volumes of distilled water, and therefore, their acidic character should not be ascribed to the acid remaining in pores after carbonization.

3.3. Thermogravimetric analysis

Figure 6A shows the TG and DTG plots for raw pork bone. The TG profile coincides with others reported in the literature for animal bones (Deydier, Guilet, Sarda, & Sharrock, 2005; Dimovic et al., 2009). The weight loss is characterized by two peaks, ascribable to a first and intense devolatilization, followed by a second and shallow one. The first step (about 40% of mass loss), in the temperature range of 50 - 200 ºC, is attributed to adsorbed water and volatile matter evaporation. The second step (about 20% of mass loss) observed between 180 and 400 ºC, is attributed to the evaporation of low molecular weight organic compounds and/or to the decomposition of collagen. Based on these results, a precarbonization temperature of 450 ºC was established, in order to cover those two peaks and remove the organic material, while retaining most of the inorganic matrix. An additional weight loss occurred gradually from 400 to 750 ºC, representing about 10% of weight. In this stage the remaining organic matter is decomposed to H_2O, CO_2, etc. At the maximum temperature of 1000 ºC, the inorganic residue still available represents about 30% of the initial mass.

The mechanism of acid activation was investigated by TG-MS analysis. Impregnated samples were heated and pyrolysis products were analysed by mass spectrometry. Figures 6B,C show the TG and DTG plots of the precursor and both acid impregnated precursor samples (before being carbonized at 800 ºC). The total weight loss at 1000 ºC increases from 30% for non activated sample to around 60% for both acid activated samples. The weight loss at around 100 ºC is caused by the desorption of adsorbed water, as confirmed in Figure 7. In the second region of weight loss (200 – 500 ºC) acid treatment caused a significant drop in the starting temperature of decomposition, which fell down from 300 ºC required for BCO to 200 ºC for acid treated samples. In this region, the DTG curve shows an intense weight loss peak for all

samples, with its maximum at around 430 ºC. The intensity of the main peak is around twice for BCP, as compared to BCO and BCS samples: the percentage of weight loss is 20, 37 and 47% for BCO, BCS and BCP, respectively. Additionally, acid activated samples show two secondary peaks at 250 and 350 ºC.

A special feature of H_2SO_4 activation is the existence of a pronounced weight loss at high temperature (above 700 ºC). This weight loss, not observed in the other samples, should be associated with gasification reactions, and could be ascribed to two possible reasons: (i) the occurrence of reactions that do not take place in the rest of the samples or, (ii) the occurrence of similar decomposition reactions as in BCP but at higher temperatures. These hypotheses were further investigated by MS analysis and are discussed below.

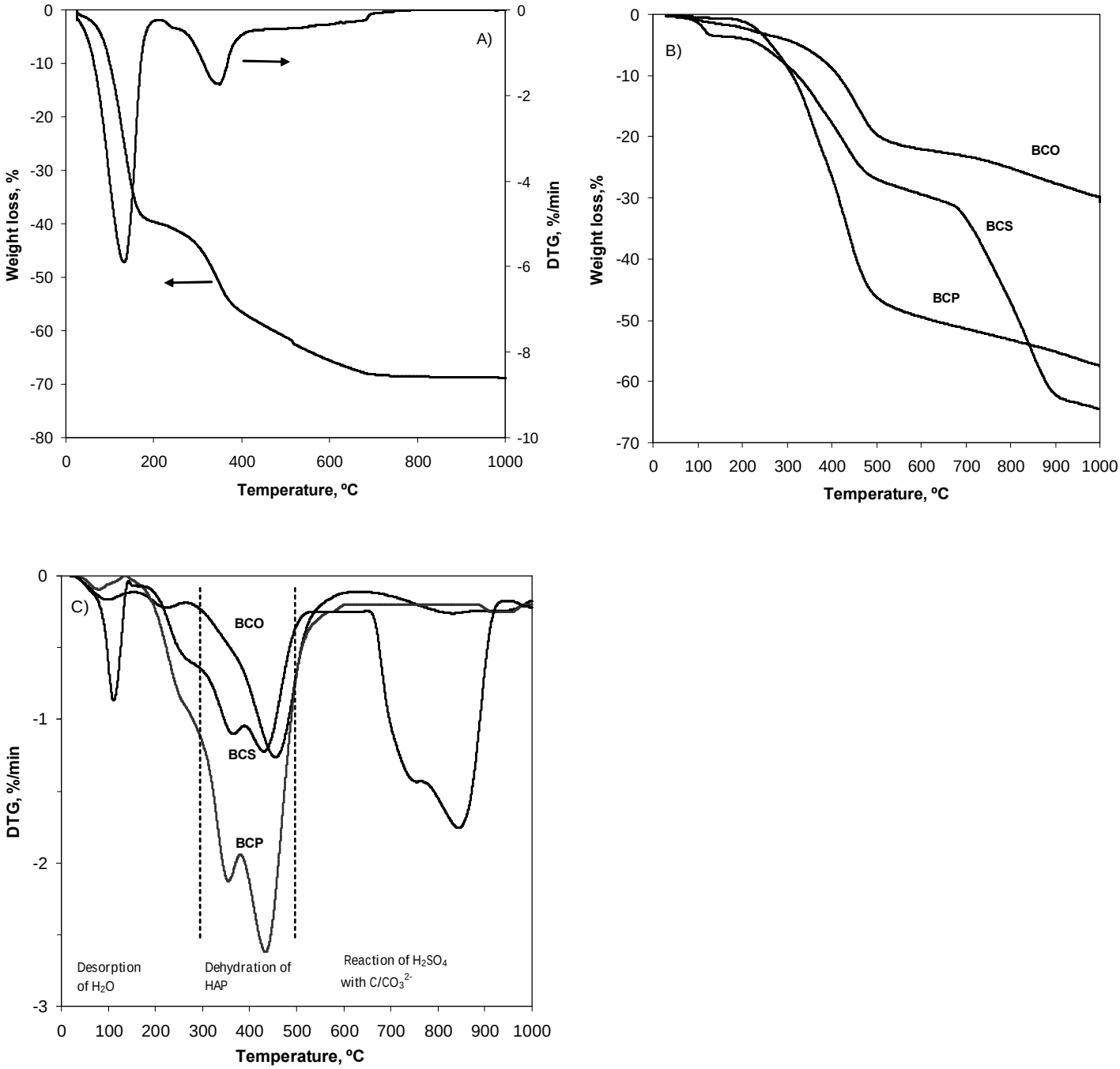

Figure 6. Thermal behaviour of different materials under He atmosphere. a) Raw pork bone; b) TG profiles of the precursor and chemically activated samples (without being carbonized at 800 ºC); c) DTG profiles of the precursor and chemically activated samples (without being carbonized at 800 ºC).

3.4. Analysis of H_2O and CO_2 release

The interaction between the acid incorporated in the impregnation stage and the constituents of the precursor (precarbonized bone char) implies reactions in which gaseous products are released. The development of porosity in bone char by chemical activation is associated with gasification reactions (U. Iriarte-Velasco, Ayastuy, Zudaire, & Sierra, 2014; Puziy et al., 2003). Regarding the precursor, calcium hydroxyapatite is the main component of bones. It is assumed that about 10% of bone char is carbon, about 8% $CaCO_3$ and the rest mainly HAp (C. W. Cheung et al., 2001).

Figure 7 shows the release of H_2O and CO_2 during the thermal treatment. The small peak of H_2O below 200 ºC (Fig. 6A) is ascribed to the desorption of adsorbed H_2O. Both acid treated samples show a large and similar release of H_2O, starting at a temperature around 350 ºC. This continuous release of H_2O (with its maximum around 475 ºC) could be related to cation-deficient HAp, described by the formula $Ca_{10-X}(HPO_4)_X(PO_4)_{6-X}(OH)_{2-X}$, formed by the acid treatment (Elliott, 1994). It is well known that at temperatures above 200 ºC the dehydration of cation-deficient HAp occurs through the decomposition of surface P-OH functionalities and phosphates (Bett, Christner, & Hall, 1967).

$$2\ \text{P-OH} \leftrightarrow \text{P-O-P} + H_2O(g) \quad (11)$$

$$HPO_4^{2-} \leftrightarrow \tfrac{1}{2} P_2O_7^{4-} + \tfrac{1}{2} H_2O(g) \quad (12)$$

The $P_2O_7^{4-}$ ion formed by reaction (12) can then react with OH^- ions at high temperatures, as given by Eq. 13 (Dimovic et al., 2009). The shoulder around 730 ºC observed in Figure 7A would correspond to H_2O formed through this reaction.

$$P_2O_7^{4-} + 2\ OH^- \leftrightarrow 2\ PO_4^{3-} + H_2O(g) \quad (13)$$

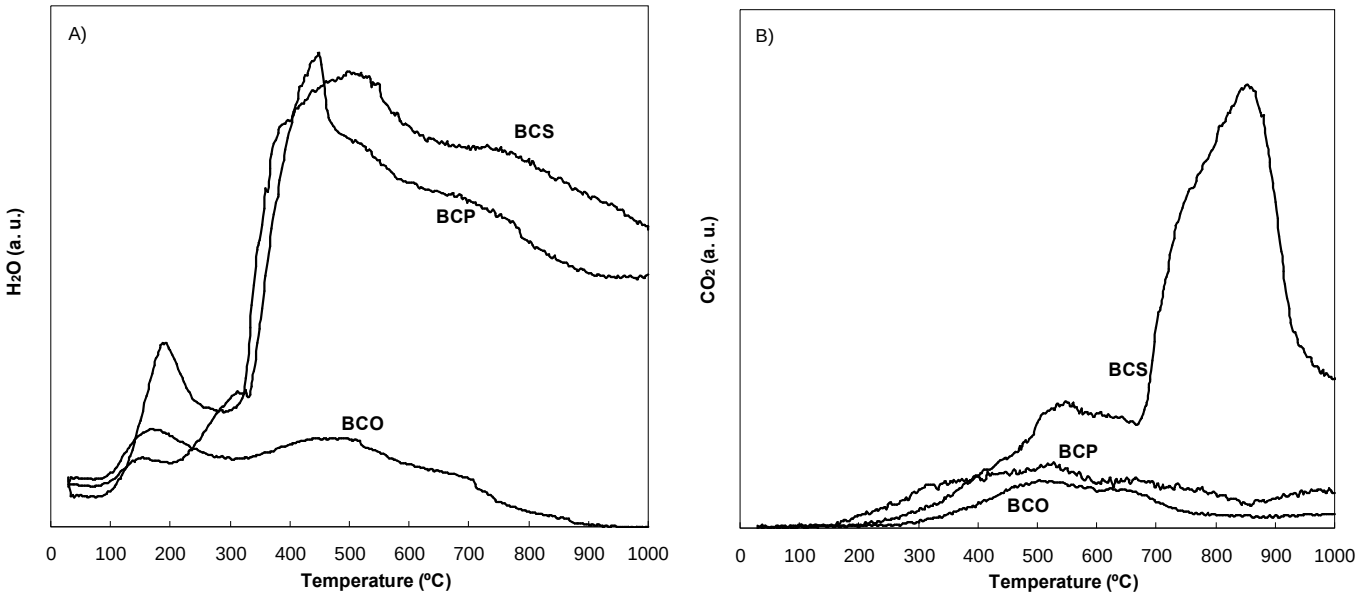

Figure 7. Intensity of mass spectrometric signals of pyrolysis products of impregnated samples (without being carbonized at 800 ºC). a) H_2O; b) CO_2.

For non activated sample (BCO) the unique dehydration reaction is given by equation (11) and causes minimal H_2O release. On the contrary, dehydration is strongly promoted by both acids. These results suggest that large amounts of ions provided by the activating agents were incorporated to produce cation-deficient HAp. In this substitution mechanism some OH^- and Ca^{+2} ions would be lost to retain charge balance, thus resulting in a lower Ca/P ratio. According to the obtained Ca/P ratios, treatment with sulphuric acid leads to the highest removal of calcium (Ca/P lowered to 0.54).

Thereafter, cation-deficient HAp would readily decompose upon thermal treatment through reactions (12) and (13), yielding the observed amorphous structure of chemically activated samples (Fig 4). The larger weight loss of acid treated samples in the 200-500 ºC range, observed in the TG plot (Fig. 5) could be therefore mainly ascribed to HAp decomposition upon chemical activation. The aforementioned reactions imply the gasification of several species and thus, are expected to take part in pore generation.

The release of CO_2 is shown in Figure 7B. All samples exhibit a band of CO_2 between 200 and 700 ºC, attributed to the reaction of carbonate ions with water (Yasukawa, Kandori, & Ishikawa, 2003).

$$CO_3^{2-} + H_2O \leftrightarrow HCO_3^- + OH^- \quad (14)$$

$$HCO_3^- \leftrightarrow CO_2 + OH^- \quad (15)$$

It is observed that chemical activation by H_2SO_4 increases CO_2 release. It is hypothesized that the reaction of H^+ ions with carbonates promotes the formation of HCO_3^- ions (Eq. 16), which are then decomposed to produce CO_2.

$$CO_3^{2-} + H^+ \leftrightarrow HCO_3^- \quad (16)$$

This behaviour cannot be observed for the sample treated with H_3PO_4. One possible explanation is that most carbonates were removed during the impregnation step, prior to thermal treatment, thus being unavailable to react. Data of Figure 4 (FTIR spectra) confirm this hypothesis. It is observed that both the precursor and BCO sample exhibit a band at 1420-1463 cm^{-1}, corresponding to the C-O stretching mode of carbonates. It is evident the absence of this band in the case of BCP, which confirms the removal of carbonates during the treatment with phosphoric acid.

The sample impregnated with sulphuric acid shows an additional peak of CO_2, in the 700 – 1000 ºC range (Fig. 7B), which cannot be observed for the other samples. This release is accompanied by a severe weight loss (Fig. 6C) and thus, should be attributed to specific gasification reactions involving carbonaceous constituents and sulphuric acid. The source of carbon could be either the carbon contained within the precursor structure or $CaCO_3$, constituent of bone char:

$$2\ H_2SO_4 + C \leftrightarrow CO_2 + 2\ SO_2 + 2\ H_2O \quad (17)$$

$$H_2SO_4 + CaCO_3 \leftrightarrow CaSO_4 + CO_2 + H_2O \quad (18)$$

On the contrary, BCP sample did not show this behaviour. There are two possible explanations: (i) that the required component for CO_2 release was removed during the acid treatment prior to thermal activation, or (ii) that phosphoric acid cannot react with the carbonaceous content of the precursor.

To summarize, it is hypothesized that CO_2 is released from the interaction between acid and calcium carbonate and/or carbon in the precursor, whereas H_2O is mainly released from the interaction of acid with HAp constituent. Since the proposed reaction mechanisms imply the gasification of constituents of bone char, they are expected to have an impact on the development of porosity.

The increased microporosity of BCS should be associated to a specific set of reactions, since the other samples do not show this behaviour. Among the reaction sets which could enhance microporosity, the reaction of H_2SO_4 with a source of carbon (Eq. 17-18) should be highlighted, according to its relative importance (measured by weight loss intensity and velocity in TG and DTG plots).

3.5. Summary of the effect of the acid treatment

The treatment with H_2SO_4 results in the partial dissolution of HAp, thus implying the formation of calcium sulphate and cation-deficient HAp, $Ca_{10-X}(HPO_4)_X(PO_4)_{6-X}(OH)_{2-X}$. This treatment involves a decrease in the Ca/P ratio, as measured by EDX. Whereas the precursor has a Ca/P ratio of 1.64 (near from the stoichiometric value of pure HAp), BCS sample exhibits a value of 0.54. This low value (very far from that of HAp) suggests that other compounds (such as calcium sulphate) coexist with hydroxyapatite in the solid phase. The presence of HAp is confirmed by XRD analysis (Figure 5), since its characteristic peaks still remain. Moreover, the FTIR analysis confirms the presence of phosphate groups (Figure 4).

The activation with sulphuric acid has also the effect of removing $CaCO_3$, constituent of bone char (Eqs. (16), (15) and (18)), which has been confirmed by FTIR and XRD analyses (Figures 4-5). Concerning the structure of the material, according to the SEM images (Figure 2), the morphology and texture of particles do not change significantly. The XRD analysis shows a slight change in the crystallinity of the material, presumably because of the presence of other solid compounds, such as calcium sulphate.

The chemical activation with H_3PO_4 has a much more aggressive effect. The XRD analysis (Figure 5) shows an amorphous structure, with only a wide band, different from those of HAp. That band could be ascribed to the coalescence of peaks corresponding to various phosphates, such as $CaHPO_4 \cdot 2H_2O$, $Ca(H_2PO_4)_2 \cdot H_2O$ and $Ca_3(PO_4)_2$), formed after the acid and heat treatment. The FTIR analysis shows several small bands (Figure 4), ascribed to phosphates. The Ca/P ratio, measured by EDX (Table 3), has also been changed (is 1.05 whereas the value of the precursor is 1.64). The activation with phosphoric acid has also the effect of removing $CaCO_3$ from bone char, as confirmed by FTIR and XRD analyses (Figures 4 and 5).

The SEM images (Figure 2) confirm the extremely aggressive effect of H_3PO_4. The acid treatment results in a significant cracking of precursor particles, since it is observed the presence of a large number of small particles. These results suggest the formation of an amorphous and thermolabile structure, which would collapse during the thermal treatment. This hypothesis is confirmed by the results of N_2 adsorption/desorption (Table 2) and production yield (Table 1). The treatment with H_3PO_4 leads to a drastic depletion of pore volume and surface area, along with a severe mass loss. To summarize, the treatment with H_3PO_4 involves a dramatic change in both the structure and composition of bone char.

3.6. Methylene blue adsorption capacity

3.6.1. Equilibrium adsorption

The adsorption isotherms of MB by samples of bone char activated at different impregnation ratios were recorded and fit to Langmuir and Freundlich models. The best fit isotherm parameters are shown in Table 4. Figure 8A shows the data for the lowest and highest impregnation ratio (0.2 mmol/g and 20 mmol/g, respectively).

Experimental data evidence the formation of monolayer. The root mean square error (RMSE) values indicate that Langmuir model better represents the adsorption equilibrium of adsorbents prepared at the highest impregnation ratios (1.0 and 20 mmol/g) which is indicative of molecules no-vertically adsorbed onto the surface. On the contrary, Freundlich model better fits equilibrium data for the adsorbents prepared at the lowest impregnation ratio (0.2 mmol/g), which is indicative of a more heterogeneous distribution of active sites onto the surface. It is likely that at larger concentrations, a stronger effect of the acids favoured the washing of the functional groups onto surface during the subsequent pyrolysis of bone char.

In general, it is observed that the uptake capacity of acid activated bone char is higher than that of non treated sample. The adsorption capacity significantly varies with the applied impregnation ratio. The optimum impregnation ratio varies depending on the activating agent used. This way, the maximum adsorption capacity by H_2SO_4 activation is achieved at 1.0 mmol/g (Q_L = 61.3 mg/g), while using H_3PO_4 it is achieved at 0.2 mmol/g (Q_L = 54.3 mg/g). These values are significantly larger than the value achieved by non activated sample (Q_L= 26.6 mg/g).

When analysing the adsorption capacity, it is essential to define the pore diameter effective to retain methylene blue. MB molecule has a minimum molecular cross-section of about 0.8 nm. Considering the characteristic pore size distribution of the prepared samples, and assuming a minimum pore diameter of two times the molecular size of MB, an effective surface area (S_{eff}) has been defined. This parameter accounts for the surface area in the 1.7 to 5.0 nm pore range, corresponding to large micropores and small mesopores.

According to the data summarized in Tables 2 and 4, there is a quite good agreement between data of S_{eff} and Q_L. When the precursor is treated with sulphuric acid, an increase in the impregnation ratio leads to a decrease in S_{eff}. Thus, low impregnation ratios are advisable to improve the uptake capacity of MB. In this case, the highest adsorption capacity is obtained at 1.0 mmol/g, whose S_{eff} is close to the maximum value. The activation with phosphoric acid follows the same trend, with decreasing values of S_{eff} as the impregnation ratio is increased. For this activating agent, the maximum uptake capacity is obtained at the lowest impregnation ratio, coinciding with the highest value of S_{eff}.

Figure 8B depicts the adsorption capacity normalized per S_{eff} surface area, which allows separating the effect of porosity from the surface chemistry of the material. It is observed that the adsorption capacity per unit of surface area (q_e/S_{eff}) increases upon acid activation. These values progressively increase, as MB solution concentration increases, up to 0.94 and 2.0 mg/m^2 for H_2SO_4 and H_3PO_4 treated samples, respectively. On the contrary, non treated sample shows a constant and lower value of about 0.35 mg/m^2 independent of the solute concentration. This indicates that the treatment with H_2SO_4 or H_3PO_4, at an adequate impregnation ratio, develops new pores and increases the affinity for adsorption of bone char surface. This behaviour was confirmed by pH_{PZC} values, which confirmed that the surface of chemically activated samples was more acid.

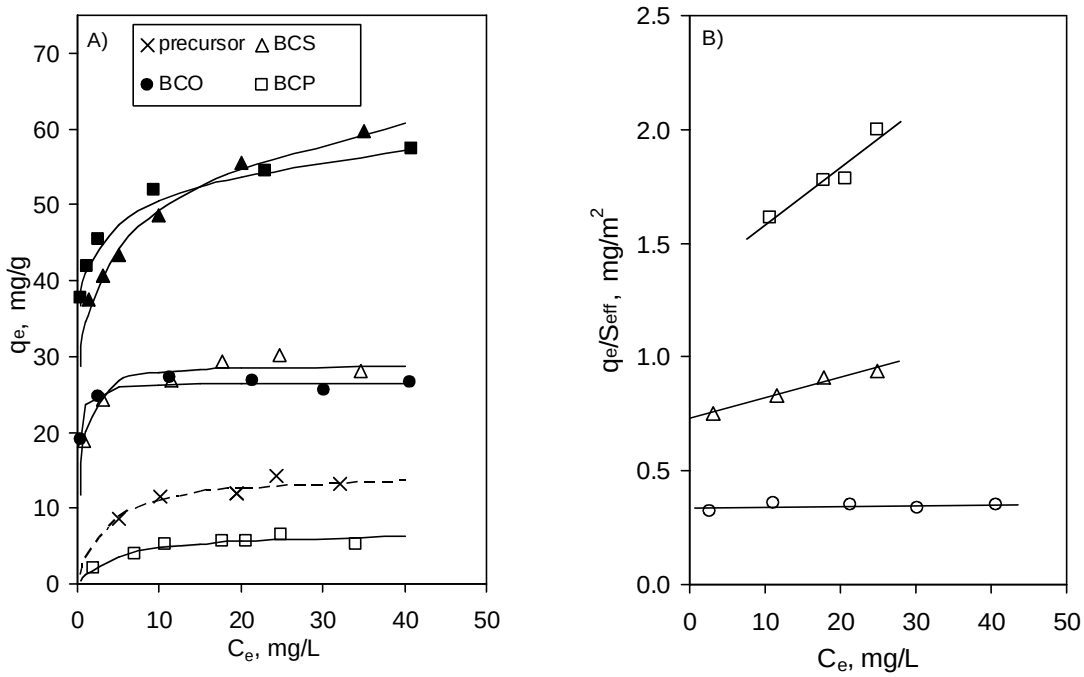

Figure 8. Equilibrium adsorption data for MB at 20 ºC and initial pH=6.0. a) Isotherm data for bone chars treated at 20 and 0.2 $mmol_{acid}/g_{precursor}$ ratio. Lines represent best model prediction; b) Isotherm data normalized per S_{eff} area. Solid symbols: r = 0.2 mmol/g; hollow symbols: r = 20 mmol/g.

Table 4. Best fit Freundlich and Langmuir isotherm parameters for MB adsorption.

	Langmuir model			Freundlich model		
	Q_L (mg/g)	b	RMSE	K_F (mg/g)·(L/mg)$^{1/n_F}$	$1/n_F$	RMSE
Precursor	14.9	0.28	0.305	6.4	0.22	0.297
BCO	26.6	8.23	0.247	22.0	0.06	0.621
BCS						
r = 20 mmol/g	29.1	2.26	0.447	20.6	0.11	0.509
r = 1.0 mmol/g	61.3	0.71	1.750	31.4	0.20	2.710
r = 0.2 mmol/g	56.7	1.03	3.596	34.6	0.15	0.814
BCP						
r = 20 mmol/g	7.15	0.20	0.369	2.0	0.33	0.374
r = 1.0 mmol/g	39.6	0.17	0.418	9.9	0.37	1.922
r = 0.2 mmol/g	54.3	3.85	2.668	41.0	0.09	0.872

3.6.2. Non-equilibrium adsorption

The adsorption time profile (Figure 9A) is similar for all adsorbents, with a gradual decline in the adsorption rate as active sites are progressively occupied. The rapid initial adsorption rate is followed by a slower increase of the amounts of solute adsorbed. Sorption equilibrium is achieved after 60 minutes for acid activated samples, whereas it takes more than 120 minutes for the precursor and non treated sample. It can be concluded that the fast phase of the process takes place within the first 20 minutes for acid treated bone chars. In this initial stage of adsorption there has been a fourfold increase in the uptake capacity by H_2SO_4 activation.

Data on Figure 9B reveal that mass transport plays an important role in the overall adsorption rate. The system dynamics was analysed by using the intraparticle diffusion model (IPDM). The initial 45 minutes of the adsorption are represented for the IPDM. When pore diffusion is implied in the overall adsorption mechanism, the representation of the fractional uptake q/q_e against the square root of the contact time is divided into two or more linear sections. These sections reflect the contribution of different mechanisms such as film diffusion and intraparticle diffusion. Figure 9B depicts that intraparticle diffusion contributes to the rate determining step. The slope of the curve gives the intraparticle diffusion rate constant (k_d) which is related to the effective diffusivity (Eq. 5). The linear plots pass close to the origin indicating that intraparticle diffusion is the dominant mechanism. It is noteworthy that acid activated samples show larger values of intercept in origin D_{eff}, reflecting that other processes such as film diffusion, also contribute to the overall uptake rate. The obtained correlation coefficients are high, above 0.98 in most cases. The best fitting values of k_d, obtained by linear regression, are summarized in Table 5. Calculated values (Eq. 5) vary in a narrow range, following the trend: BCO ≥ BCP ≥ Precursor > BCS, indicating that pore diffusivity slightly decreases with H_2SO_4 activation. This behaviour is attributed to the reduction in the pore average size and the effect of counter diffusion of exchanged ions. However, the increased initial solute uptake rate led to a more efficient utilization of the adsorptive capacity of H_2SO_4 treated bone char. Analysed in conjunction with TG-MS data, these data suggest that H_2SO_4 readily reacted with the carbonaceous content of the precursor. This reaction could play an important role in the enhanced porosity of bone char.

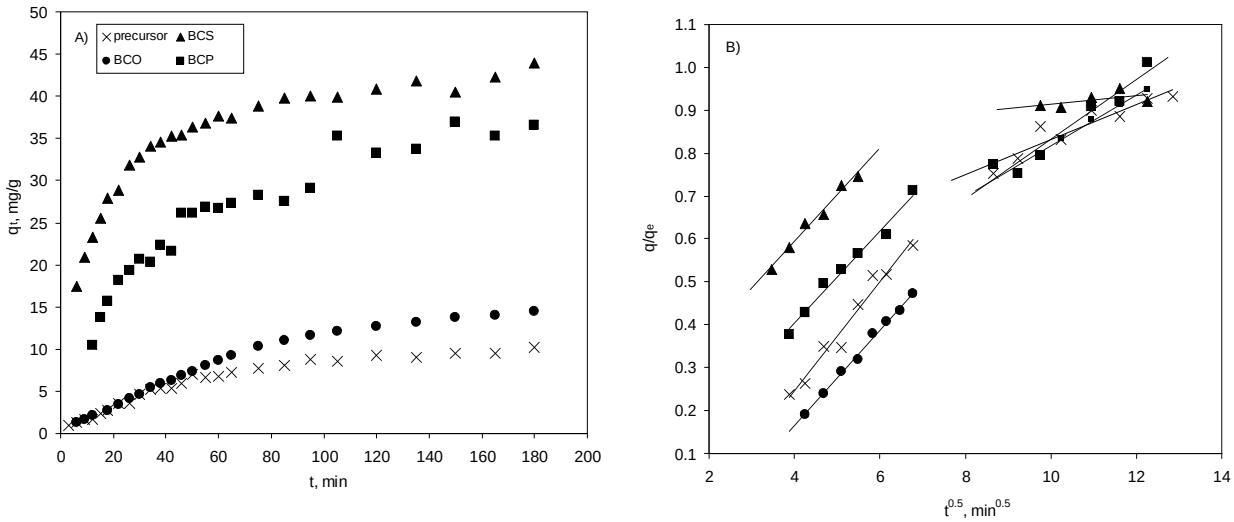

Figure 9. MB adsorption kinetics onto bone chars (r =0.2 mmol/g). Initial solute concentration= 25 mg/L; initial pH= 5.8; adsorbent mass= 10 mg. a) Adsorption time profile; b) Fitting of data to the intraparticle diffusion model (Eq. 5).

Table 5. Intraparticle diffusion constant (k_d) and diffusivity (D_{eff}) for MB adsorption at 20 °C. Initial concentration 25 mg/L, 1 g_{BC}/L.

	D_P, mm	k_d, $min^{-0.5}$	D_{eff}, cm^2/min	R^2
Precursor	0.213	0.127	$1.88 \cdot 10^{-7}$	0.9669
BCO	0.295	0.111	$2.33 \cdot 10^{-7}$	0.9955
BCP	0.289	0.107	$2.10 \cdot 10^{-7}$	0.9816
BCS	0.210	0.108	$1.04 \cdot 10^{-7}$	0.9807

4. Conclusions

A porous biochar was manufactured through the valorisation of waste pork bones. Acid treatment (by either H_2SO_4 or H_3PO_4) at the lowest impregnation ratio of 0.2 $mmol_{acid}/g_{precursor}$ increased BET area by about 80% (compared to untreated sample of bone char). When using H_2SO_4, a further increase in the impregnation ratio significantly enhanced the microporosity of the resultant material, up to 263%.

Between both acid reagents, H_3PO_4 is more active and thus, although the maximum impregnation ratio used in this work (20 mmol/g) was within the normal range used for the

acid activation of other precursors, it led to a dramatic removal of porosity, due to the collapse of pore walls. Consequently, much lower impregnation ratios are required. The values commonly used in the literature are valid for the activation with H_2SO_4.

Acid treatment (with either H_2SO_4 or H_3PO_4) led to important changes in bone char structure, which may be attributed to the formation of cation deficient HAp and its subsequent decomposition upon thermal treatment, confirmed by the release of H_2O during the pyrolysis step. Since the proposed reaction mechanism implies the gasification of constituents of bone char, it is expected to have an impact on the development of porosity. The increased microporosity of BCS should be associated to a specific set of reactions of H_2SO_4 with a source of carbon (carbon constituent of bone char or carbonates), which results in the release of CO_2.

The isotherm results revealed that the maximum uptake capacity of methylene blue was achieved after acid activation at low impregnation ratios: 1.0 mmol/g using H_2SO_4, and 0.2 mmol/g using H_3PO_4. These values were considerably larger than that of non impregnated sample, and could be related to the effective surface area, defined as surface area in the 1.7 to 5.0 nm pore range, corresponding to large micropores and small mesopores. S_{eff} normalized monolayer capacities revealed that acid treatment at suitable conditions (low impregnation ratios) also increased the density of available adsorption sites on the surface of bone char.

Acknowledgements

The authors wish to thank to the Basque Government (UFI 11/39 (UPV/EHU) and S-PE13UN100 (SAI13/254)) for their economic support.

Bibliography

Acharya, C. K., Jiang, F., Liao, C., Fitzgerald, P., Vecchio, K. S., & Cattolica, R. J. (2013). Tar and CO_2 removal from simulated producer gas with activated carbon and charcoal. *Fuel Processing Technology, 106*(0), 201-208.

Arvanitoyannis, I. S., & Ladas, D. (2008). Meat waste treatment methods and potential uses. *International Journal of Food Science & Technology*, *43*, 543-559.

Babic, B. M., Milonjic, S. K., Polovina, M. J., & Kaludierovic, B. V. (1999). Point of zero charge and intrinsic equilibrium constants of activated carbon cloth. *Carbon, 37*(3), 477-481.

Bamzai, K. K., Suri, S., & Singh, V. (2012). Synthesis, characterization, thermal and dielectric properties of pure and cadmium doped calcium hydrogen phosphate. *Materials Chemistry and Physics, 135*(1), 158-167.

Bett, J. A. S., Christner, L. G., & Hall, W. K. (1967). Hydrogen held by solids. XII. hydroxyapatite catalysts. *Journal of the American Chemical Society, 89*(22), 5535-5541.

Cascarosa, E., de Zarate, M. C. O., Sanchez, J. L., Gea, G., & Arauzo, J. (2012). Sulphur removal using char and ash from meat and bone meal pyrolysis. *Biomass & Bioenergy, 40*, 190-193.

Cheung, C. W., Chan, C. K., Porter, J. F., & McKay, G. (2001b). Combined diffusion model for the sorption of cadmium, copper, and zinc ions onto bone char. *Environmental Science and Technology, 35*(7), 1511-1522.

De la Puente, G., Pis, J. J., Menéndez, J. A., & Grange, P. (1997). Thermal stability of oxygenated functions in activated carbons. *Journal of Analytical and Applied Pyrolysis, 43*(2), 125-138.

Deydier, E., Guilet, R., Sarda, S., & Sharrock, P. (2005). Physical and chemical characterisation of crude meat and bone meal combustion residue: "waste or raw material?". *Journal of Hazardous Materials, 121*(1-3), 141-148.

Dimovic, S., Smiciklas, I., Plecas, I., Antonovic, D., & Mitric, M. (2009). Comparative study of differently treated animal bones for Co^{2+} removal. *Journal of Hazardous Materials, 164*(1), 279-287.

Elliott, J. C. (1994). Studies in Inorganic Chemistry Volume 18: Structure and chemistry of the Apatites and Other Calcium Orthophosphates. Elsevier, Amsterdam, 148-154.

Giardina, M. A., & Fanovich, M. A. (2010). Synthesis of nanocrystalline hydroxyapatite from $Ca(OH)_2$ and H_3PO_4 assisted by ultrasonic irradiation. *Ceramics International, 36*(6), 1961-1969.

Goodman, P. A., Li, H., Gao, Y., Lu, Y. F., Stenger-Smith, J. D., & Redepenning, J. (2013). Preparation and characterization of high surface area, high porosity carbon monoliths from pyrolyzed bovine bone and their performance as supercapacitor electrodes. *Carbon, 55*, 291-298.

Gumus, R., Wauton, I., & Aliu, A. (2012). Investigation of the effect of chemical activation and characterization of bone char: Cow bone. *Journal of Engineering and Applied Science, 4*, 34-45.

Iriarte-Velasco, U., Sierra, I., Zudaire, L., & Ayastuy, J. L. (2015). Conversion of waste animal bones into porous hydroxyapatite by alkaline treatment: Effect of the impregnation ratio and investigation of the activation mechanism. *Journal of Materials Science, 50*, 7568-7582.

Iriarte-Velasco, U., Ayastuy, J. L., Zudaire, L., & Sierra, I. (2014). An insight into the reactions occurring during the chemical activation of bone char. *Chemical Engineering Journal, 251*(0), 217-227.

Iriarte-Velasco, U., Sierra, I., Cepeda, E. A., Bravo, R., & Ayastuy, J. L. (2015). Methylene blue adsorption by chemically activated waste pork bones. *Coloration Technology, 131*(4), 322-332.

Izquierdo, M. T., Martínez de Yuso, A., Rubio, B., & Pino, M. R. (2011). Conversion of almond shell to activated carbons: Methodical study of the chemical activation based on an experimental design and relationship with their characteristics. *Biomass and Bioenergy, 35*(3), 1235-1244.

Jimenez-Cordero, D., Heras, F., Alonso-Morales, N., Gilarranz, M. A., & Rodriguez, J. J. (2013). Development of porosity upon physical activation of grape seeds char by gas phase oxygen chemisorption–desorption cycles. *Chemical Engineering Journal, 231*(0), 172-181.

Kon, M., Hirakata, L. M., Miyamoto, Y., Kawano, F., & Asaoka, K. (2002). Surface-layer modification of hydroxyapatite ceramic with acid and heat treatments. *Dental Materials Journal, 21*(2), 170-80.

Krupa-Żuczek, K., Kowalski, Z., & Wzorek, Z. (2008). Manufacturing of phosphoric acid from hydroxyapatite, contained in the ashes of the incinerated meat-bone wastes. *Polish Journal of Chemical Technology, 10*(3), 13-20.

Lillo-Ródenas, M. A., Cazorla-Amorós, D., & Linares-Solano, A. (2003). Understanding chemical reactions between carbons and NaOH and KOH: An insight into the chemical activation mechanism. *Carbon, 41*(2), 267-275. doi:10.1016/S0008-6223(02)00279-8

Medellin-Castillo, N. A., Leyva-Ramos, R., Padilla-Ortega, E., Perez, R. O., Flores-Cano, J. V., & Berber-Mendoza, M. S. (2014). Adsorption capacity of bone char for removing fluoride from water solution. Role of hydroxyapatite content, adsorption mechanism and competing anions. *Journal of Industrial and Engineering Chemistry, 20*(6), 4014-4021.

Ministry of Agriculture, Food and Environment (2015). El sector de la carne de cerdo en cifras. Principales indicadores económicos en 2014. Online december 2015. http://www.magrama.gob.es

Moreno-Castilla, C., Carrasco-Marin, F., Lopez-Ramon, M. V., & Alvarez-Merino, M. A. (2001). Chemical and physical activation of olive-mill waste water to produce activated carbons. *Carbon, 39*(9), 1415-1420.

Njoku, V. O., & Hameed, B. H. (2011). Preparation and characterization of activated carbon from corncob by chemical activation with H_3PO_4 for 2,4-dichlorophenoxyacetic acid adsorption. *Chemical Engineering Journal, 173*(2), 391-399.

Obadiah, A., Swaroopa, G. A., Kumar, S. V., Jeganathan, K. R., & Ramasubbu, A. (2012). Biodiesel production from palm oil using calcined waste animal bone as catalyst. *Bioresource Technology, 116*(0), 512-516.

Phan, N. H., Rio, S., Faur, C., Le Coq, L., Le Cloirec, P., & Nguyen, T. H. (2006). Production of fibrous activated carbons from natural cellulose (jute, coconut) fibers for water treatment applications. *Carbon, 44*(12), 2569-2577.

Puziy, A. M., Poddubnaya, O. I., Martínez-Alonso, A., Suárez-García, F., & Tascón, J. M. D. (2003). Synthetic carbons activated with phosphoric acid III. Carbons prepared in air. *Carbon, 41*(6), 1181-1191.

Rafatullah, M., Sulaiman, O., Hashim, R., & Ahmad, A. (2010). Adsorption of methylene blue on low-cost adsorbents: A review. *Journal of Hazardous Materials, 177*(1-3), 70-80.

Reffas, A., Bernardet, V., David, B., Reinert, L., Lehocine, M. B., Dubois, M., et al. (2010). Carbons prepared from coffee grounds by H_3PO_4 activation: Characterization and adsorption of methylene blue and nylosan red N-2RBL. *Journal of Hazardous Materials, 175*(1–3), 779-788.

Reyes-Gasga, J., Martínez-Piñeiro, E. L., Rodríguez-Álvarez, G., Tiznado-Orozco, G. E., García-García, R., & Brès, E. F. (2013). XRD and FTIR crystallinity indices in sound human tooth enamel and synthetic hydroxyapatite. *Materials Science and Engineering: C, 33*(8), 4568-4574.

Rezaee, A., Ghanizadeh, G., Behzadiyannejad, G., Yazdanbakhsh, A., & Siyadat, S. D. (2009). Adsorption of endotoxin from aqueous solution using bone char. *Bulletin of Environmental Contamination and Toxicology, 82*(6), 732-737.

Šljivić-Ivanović, M., Smičiklas, I., Milenković, A., Dojčinović, B., Babić, B., & Mitrić, M. (2015). Evaluation of the effects of treatment factors on the properties of bio-apatite materials. *Journal of Materials Science, 50*(1), 354-365.

Wei, S., Zhang, H., Huang, Y., Wang, W., Xia, Y., & Yu, Z. (2011). Pig bone derived hierarchical porous carbon and its enhanced cycling performance of lithium-sulfur batteries. *Energy & Environmental Science, 4*(3), 736-740.

Yasukawa, A., Kandori, K., & Ishikawa, T. (2003). TPD-TG-MS study of carbonate calcium hydroxyapatite particles. *Calcified Tissue International, 72*(3), 243-250.

Yusufu, M. I., Ariahu, C. C., & Igbabul, B. D. (2012). Production and characterization of activated carbon from selected local raw materials. *African Journal of Pure and Applied Chemistry, 6*(9), 123-131.

Zendah, H., Khattech, I., & Jemal, M. (2013). Thermochemical and kinetic studies of the acid attack of "B" type carbonate fluorapatites at different temperatures (25–55)°C. *Thermochimica Acta, 565*(0), 46-51.

Figure captions

Figure 1. Pore distribution of acid treated bone chars. a) Treatment with sulphuric acid; b) Treatment with phosphoric acid.

Figure 2. SEM images of the prepared bone chars.

Figure 3. Local EDX spectra of prepared bone chars.

Figure 4. FTIR spectra of the precursor and acid treated samples.

Figure 5. XRD patterns for the precursor and acid treated samples.

Figure 6. Thermal behaviour of different materials under He atmosphere. a) Raw pork bone; b) TG profiles of the precursor and chemically activated samples (without being carbonized at 800 ºC); c) DTG profiles of the precursor and chemically activated samples (without being carbonized at 800 ºC).

Figure 7. Intensity of mass spectrometric signals of pyrolysis products of impregnated samples (without being carbonized at 800 ºC). a) H_2O; b) CO_2.

Figure 8. Equilibrium adsorption data for MB at 20 ºC and initial pH=6.0. a) Isotherm data for bone chars treated at 20 and 0.2 $mmol_{acid}/g_{precursor}$ ratio. Lines represent best model prediction; b) Isotherm data normalized per S_{eff} area. Solid symbols: r = 0.2 mmol/g; hollow symbols: r = 20 mmol/g.

Figure 9. MB adsorption kinetics onto bone chars (r =0.2 mmol/g). Initial solute concentration= 25 mg/L; initial pH=5.8; adsorbent mass= 10 mg. a) Adsorption time profile; b) Fitting of data to the intraparticle diffusion model (Eq. 5).